NEUROSCIENCE

Thermosensitive receptors in neural stem cells link stress-induced hyperthermia to impaired neurogenesis via microglial engulfment

Yutaka Hoshi[1], Koji Shibasaki[2], Philippe Gailly[3], Yuji Ikegaya[1,4,5], Ryuta Koyama[1]*

Social stress impairs hippocampal neurogenesis and causes psychiatric disorders such as depression. Recent studies have highlighted the significance of increased body temperature in stress responses; however, whether and how social stress–induced hyperthermia affects hippocampal neurogenesis remains unknown. Here, using transgenic mice in which the thermosensitive transient receptor potential vanilloid 4 (TRPV4) is conditionally knocked out in Nestin-expressing neural stem cells (NSCs), we found that social defeat stress (SDS)–induced hyperthermia activates TRPV4 in NSCs in the dentate gyrus and thereby impairs hippocampal neurogenesis. Specifically, SDS activated TRPV4 in NSCs and induced the externalization of phosphatidylserine in NSCs, which was recognized by the brain-resident macrophage, microglia, and promoted the microglial engulfment of NSCs. SDS-induced impairment of hippocampal neurogenesis was ameliorated by NSC-specific knockout of TRPV4 or pharmacological removal of microglia. Thus, this study reveals a previously unknown role of thermosensitive receptors expressed by NSCs in stress responses.

INTRODUCTION

Social stress has been shown to impair neurogenesis in the hippocampal dentate gyrus (DG), which could result in maladaptive behavior (*1*, *2*). Recent studies have shown that social stress induces core hyperthermia and maladaptive behavior (*3*, *4*). Changes in core temperature correlate with changes in brain temperature (*5*, *6*), and even slight changes in brain temperature could affect brain function (*7*, *8*). However, it remains unclear whether and how stress-induced hyperthermia affects hippocampal neurogenesis.

To address this question, we investigated the possible involvement of the thermosensitive transient receptor potential vanilloid 4 (TRPV4) in impairment of hippocampal neurogenesis in a mouse model of social defeat stress (SDS). TRPV4 is a nonselective cation channel that is activated at approximately body temperature (>27° to 34°C) (*9*, *10*) and modulates both neuronal and glial functions in the brain (*11*, *12*). Furthermore, it has been shown that *Trpv4* mRNA is highly expressed in the hippocampus (*10*). These findings motivated us to investigate the role of TRPV4 as a mediator linking SDS-induced hyperthermia and SDS-induced impairment of hippocampal neurogenesis.

Here, we found that expression of TRPV4 in Nestin-expressing neural stem cells (NSCs) in the subgranular zone (SGZ) of the DG is higher than that in other cell types in the hippocampus. Establishing a transgenic mouse line in which TRPV4 is conditionally knocked out in NSCs, we found that TRPV4 expressed by hippocampal NSCs mediates SDS-induced impairment of hippocampal neurogenesis. Furthermore, we found that activation of TRPV4 in NSCs promotes the externalization of phosphatidylserine (PS) on NSCs, which is recognized by the brain-resident macrophage microglia and enhances microglial engulfment of NSCs. Together, our findings revealed a previously unknown mechanism by which stress-induced hyperthermia impairs hippocampal neurogenesis through activation of TRPV4 in NSCs.

[1]Laboratory of Chemical Pharmacology, Graduate School of Pharmaceutical Sciences, The University of Tokyo, Tokyo 113-0033, Japan. [2]Laboratory of Neurochemistry, Graduate School of Human Health Science, University of Nagasaki, Nagasaki 851-2195, Japan. [3]Laboratory of Cell Physiology, Institute of Neuroscience, Université catholique de Louvain, B-1200 Brussels, Belgium. [4]Institute for AI and Beyond, The University of Tokyo, Tokyo 113-0033, Japan. [5]Center for Information and Neural Networks, National Institute of Information and Communications Technology, Suita City, Osaka 565-0871, Japan.
*Corresponding author. Email: rkoyama@mol.f.u-tokyo.ac.jp

RESULTS

TRPV4 mediates SDS-induced neurogenesis impairment

In this study, we used a mouse model of SDS (*13*, *14*) with minor modifications, in which a C57BL/6J mouse or a transgenic mouse with C57BL/6J backgrounds (male, 4 weeks old) was placed in the novel cage with an aggressor ICR mouse (male, 8 to 10 weeks old) (Fig. 1A). Because the surface body temperatures of the defeated mice were elevated compared to naïve mice that did not receive SDS (Fig. 1B), we quantitatively measured the rectal temperature as an indicator of core temperature and found that the core temperature increased after defeat (Fig. 1C). It has been shown that increases in core temperature correlate with increases in brain temperature (*5*, *6*), and this finding was confirmed in the present study (fig. S1, A to C). Furthermore, SDS induced depressive behavior in the tail suspension test (TST) and anxious behavior in the elevated plus maze test (EPMT), supporting the validity of the SDS model used in this study (fig. S2, A to D).

Next, we assessed whether SDS influences adult hippocampal neurogenesis through activation of TRPV4, a thermosensitive nonselective cation channel (*9*, *10*), to examine the role of temperature signals in the brain. TRPV4 deficiency did not affect the SDS-induced increase in core temperature (Fig. 1C). To label newborn cells in the DG, we intraperitoneally injected wild-type (WT) or TRPV4 knockout (KO) mice with 5-ethynyl-2′-deoxyuridine (EdU; Fig. 1A), which is taken up only by dividing cells. Immunohistochemical analysis showed that EdU^+ cells were immunopositive for both doublecortin (DCX; a marker of immature neurons) and Prox1 (a marker of dentate granule cells) in the SGZ of the DG (Fig. 1D). The density of $Prox1^+$ neurons was not substantially different between naïve and SDS mice [naïve, $16.227 \pm 0.391 \times 10^3$ cells/mm^2; SDS, $15.954 \pm 0.408 \times 10^3$ cells/mm^2; $P = 0.645$, Student's t test; $n = 5$ and 6 mice

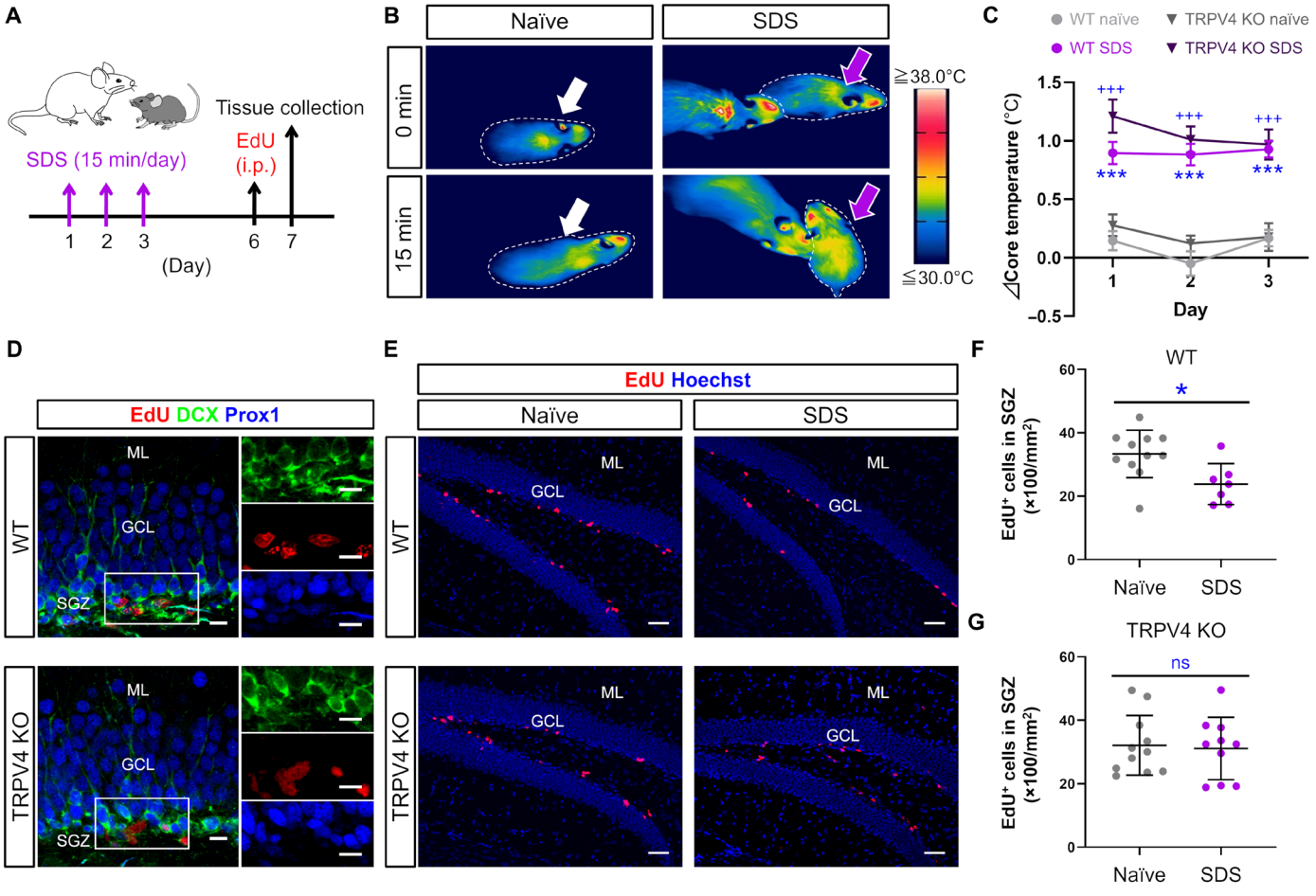

Fig. 1. TRPV4 mediates hippocampal neurogenesis impairment. (**A**) Schedule of the experiment in which newborn cells were labeled with EdU after SDS. i.p., intraperitoneally. (**B**) Infrared thermal imaging indicated that body temperature was elevated in SDS-subjected mice (purple arrows). The white arrows indicate mice not exposed to SDS (naïve). Each mouse is indicated with dashed lines. (**C**) SDS-induced core temperature elevation in WT and TRPV4 KO mice. $n = 21$ (naïve WT), 22 (SDS-exposed WT), 23 (naïve TRPV4 KO), and 23 (SDS-exposed TRPV4 KO) mice. (**D**) Confocal images of Prox1 and DCX immunostaining in the DG. EdU-positive newborn cells expressed Prox1 and DCX in WT and TRPV4 KO mice. Inset, SGZ. Scale bars, 10 μm. (**E**) Representative confocal images of EdU-labeled cells (red) in the DG. Scale bars, 50 μm. (**F** and **G**) The number of newborn cells in the SGZ was decreased in SDS group. This decrease was not observed in TRPV4 KO group. $n = 12$ (naïve WT), 7 (SDS-exposed WT), 11 (naïve TRPV4 KO), 10 (SDS-exposed TRPV4 KO) mice; four areas from two to three sections, from each mouse. All n values refer to the number of mice used. $^{*}P < 0.05$ and $^{***}P < 0.001$ versus naïve WT mice; $^{+++}P < 0.001$ versus naïve TRPV4 KO mice, Student's t test (F and G) or one-way analysis of variance (ANOVA) followed by Tukey-Kramer's post hoc test (C). Data are means ± SEM. ns, not significant.

(four areas per mouse), respectively], suggesting that SDS does not affect total neuron number. Consistent with previous studies, SDS reduced the number of EdU^+ cells in the DG in WT mice (Fig. 1, E and F). In contrast, this effect was suppressed in TRPV4 KO mice (Fig. 1, E and G). These results suggest that SDS-induced TRPV4 activation is responsible for the reduction in neurogenesis in the DG.

TRPV4 activation in Nestin-expressing NSCs regulates SDS-induced abnormality

Previous studies have shown that TRPV4 is expressed in neurons, astrocytes, and microglia in the brain (*10*, *15*–*17*). In this study, we generated an anti-TRPV4 antibody (fig. S3, A and B) and examined TRPV4 expression in the hippocampus by immunostaining. We found that the TRPV4 protein was expressed in the DG (fig. S4A), which is the hippocampal neurogenic niche, and colocalized with Nestin, a molecular marker of NSCs (Fig. 2A), suggesting that TRPV4 is highly expressed in NSCs. TRPV4 expression was clearly observed in the radial processes of NSCs extending toward granule cells. The expression of TRPV4 and coexpression with Nestin were hardly detected in TRPV4 KO mice, supporting the validation of the antibody we used (Fig. 2B). Double immunostaining for TRPV4 and NeuN (neuronal marker), S100β (astrocytic marker), or Iba1 (microglial marker) showed that TRPV4 is expressed in these cells at lower levels than in Nestin-expressing NSCs (figs. S4, B and C).

Therefore, we investigated the mechanism by which activation of TRPV4 in NSCs mediates SDS-induced impairment of neurogenesis. For this purpose, we established a triple-transgenic mouse line with the tamoxifen-inducible Cre-*loxP* system driven by the *Nestin* promoter. This mouse line carries *loxP*-flanked *Trpv4* alleles ($Trpv4^{fl/fl}$), tamoxifen-inducible $Nestin\text{-}CreER^{T2}$, and an *R26R-CAG-loxP-flanked-tdTomato* (*RCL-tdTomato*) reporter (Fig. 2C). In these mice, TRPV4 is deleted, and tdTomato is specifically expressed

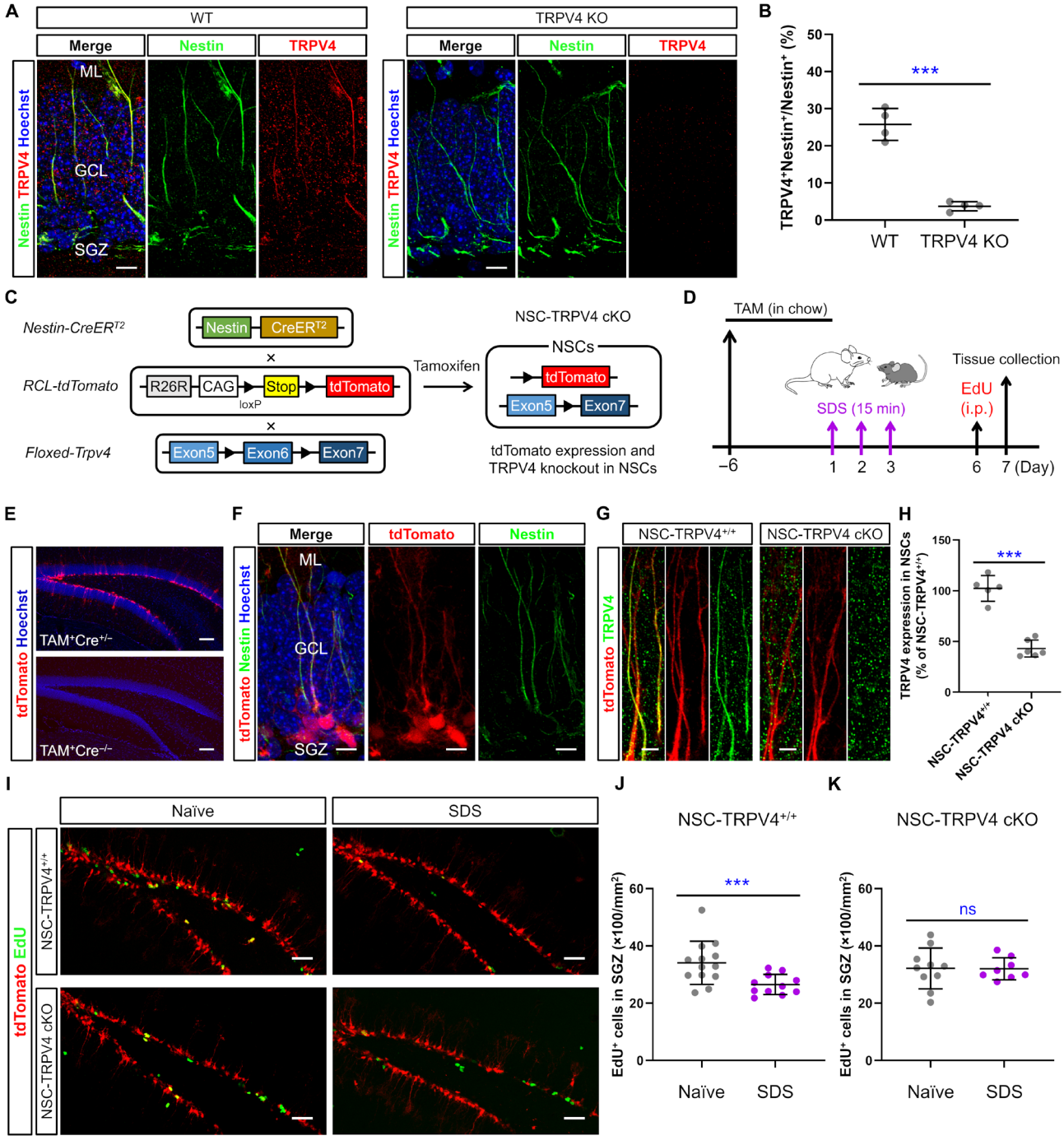

Fig. 2. TRPV4 in NSCs mediates SDS-induced impairment of neurogenesis. (**A**) Confocal analysis of TRPV4 and Nestin coexpression in the DG. Nuclei (blue) were counterstained with Hoechst 33342. ML, molecular layer; GCL, granule cell layer. Scale bar, 10 μm. (**B**) TRPV4 was hardly detected in TRPV4 KO mice, supporting the validity of the antibody used in this study. $n = 3$ mice; four areas from two to three sections from each mouse. ***$P < 0.05$, Mann-Whitney rank sum test. Data are means ± SEM. (**C**) Breeding strategy for inducing specific deletion of TRPV4 and expression of tdTomato in NSCs. (**D**) Schedule of tamoxifen treatment and histological analysis. (**E**) Confocal images of NSCs (red) in the DG after 1 week of tamoxifen treatment. tdTomato was not expressed in $Cre^{-/-}$ mice, indicating that precise recombination occurred. Scale bars, 100 μm. (**F**) Confocal images of tdTomato (red) and Nestin (green), indicating that Nestin was expressed in NSCs in NSC-$TRPV4^{+/+}$ mice. Scale bars, 10 μm. (**G**) Confocal images of tdTomato (red) and TRPV4 (green) in the DG. Scale bars, 5 μm. (**H**) TRPV4 expression in NSCs was down-regulated in NSC-TRPV4 cKO mice. $n = 5$ (NSC-$TRPV4^{+/+}$) and 6 (NSC-TRPV4 cKO) mice; four areas from two to three sections from each mouse. (**I**) Representative confocal images of NSCs (red) and newborn cells (green) in the DG in NSC-$TRPV4^{+/+}$ and NSC-TRPV4 cKO mice. Scale bars, 50 μm. (**J** and **K**) The number of newborn cells was decreased in SDS-exposed NSC-$TRPV4^{+/+}$ mice. This decrease was not observed in NSC-TRPV4 cKO mice. $n = 10$ (naïve NSC-$TRPV4^{+/+}$), 10 (SDS-exposed NSC-$TRPV4^{+/+}$), 10 (naïve NSC-TRPV4 cKO), and 8 (SDS-exposed NSC-TRPV4 cKO) mice; four areas from two to three sections from each mouse. All n values refer to the number of mice used. ***$P < 0.001$ versus naïve NSC-$TRPV4^{+/+}$ mice, Student's t test. Data are means ± SEM.

in NSCs. The mice used in the present study were designated *Nestin-CreER^{T2}::RCL-tdTomato::Trpv4$^{fl/fl}$* [NSC-TRPV4 conditional KO (cKO)] mice and *Nestin-CreER^{T2}::RCL-tdTomato* (NSC-TRPV4$^{+/+}$) mice (as controls). The mice were fed tamoxifen chow for 1 week to induce Cre-mediated deletion of TRPV4 and tdTomato expression (Fig. 2, D to F). Immunohistochemical analysis confirmed that TRPV4 expression was down-regulated in NSCs in the DG in NSC-TRPV4 cKO mice compared to NSC-TRPV4$^{+/+}$ mice (Fig. 2, G and H). In NSC-TRPV4 cKO mice, SDS-induced hyperthermia was not affected (fig. S5), whereas impairment of neurogenesis was suppressed (Fig. 2, I to K). Collectively, these results suggest that SDS-induced impairment of neurogenesis is mediated by TRPV4 in NSCs.

Microglia mediate SDS-induced impairment of neurogenesis

Next, we examined the mechanism by which TRPV4 activation in NSCs causes neurogenesis impairment. Because accumulating evidence suggests that microglia play an important role in the regulation of neurogenesis in health and disease (*18*–*20*), we focused on microglia, which are brain-resident macrophages. First, we performed immunostaining for Iba1, a marker of microglia, and CD68, a marker of lysosomes and is required for phagocytosis (Fig. 3A). SDS increased the volume of microglial CD68 staining in WT mice, but this increase was suppressed in TRPV4 KO mice (Fig. 3, B to E). These results suggest that the activation of TRPV4 by SDS mediates the enhancement of phagocytosis.

Next, to directly investigate the involvement of microglia in SDS-induced impairment of neurogenesis, we depleted microglia in mice by administering the CSF1R/c-kit inhibitor PLX3397 (Fig. 3, F and G). SDS-induced hyperthermia was maintained in PLX3397-treated mice (Fig. 3H). We then examined SDS-induced neurogenesis impairment in PLX3397-treated mice. We found that microglial depletion suppressed SDS-induced neurogenesis impairment (Fig. 3, I to K). It should be noted that the pharmacological removal of microglia by PLX3397 is nonspecific in at least two ways. First, PLX3397 removes not only nonmicroglial macrophages in the brain but also macrophages in the periphery. Second, because the administration of PLX3397 removes microglia from the entire brain, this approach cannot rule out the effect of TRPV4-independent microglial function on neurogenesis.

We then examined whether the engulfment of NSCs by microglia is induced in a TRPV4-dependent manner. Immunostaining for NSCs (tdTomato), microglia (Iba1), and microglial lysosomes (CD68) revealed that both the volume of CD68 staining (Fig. 4A) and microglial engulfment of NSCs (indicated by tdTomato signals in microglial CD68 signals; Fig. 4B and movie S1) were increased in NSC-TRPV4$^{+/+}$ mice (Fig. 4, C and E), whereas these phenomena were suppressed in NSC-TRPV4 cKO mice (Fig. 4, D and F).

Furthermore, to assess when microglial engulfment of NSCs starts after SDS, NSC-TRPV4$^{+/+}$ and NSC-TRPV4 cKO mice underwent a single SDS paradigm, and tissues were collected 2 hours later for immunohistochemistry (fig. S6A). The SDS-induced increase in the volume of microglial CD68 staining and phagocytosis of NSCs was promoted 2 hours after a single SDS paradigm (fig. S6, B to E). These results suggest that the SDS-induced increase in the phagocytic activity of microglia starts no later than 2 hours after SDS and may have a long-term impact on hippocampal neurogenesis. Collectively, these results suggest that SDS-induced impairment of neurogenesis is mediated by TRPV4 in NSCs and engulfment of NSCs by microglia.

TRPV4 activation promotes microglial engulfment of NSCs via externalized PS recognition

Next, we examined how activation of TRPV4 promotes engulfment of NSCs by microglia. Because TRPV4 is a Ca^{2+}-permeable nonselective cation channel, we focused on the involvement of PS, which is extracellularly exposed upon increases in intracellular Ca^{2+} levels and acts as an "eat me" signal (*21*–*23*). First, we investigated whether externalization of PS on NSCs is increased by SDS using the fluorescently labeled PS-binding probe PSVue. We found that SDS promoted the externalization of PS in NSCs in a TRPV4-dependent manner (Fig. 5, A to C).

Next, to visualize the interaction between PS exposed on NSCs and microglia, we generated quadruple transgenic mice by crossing NSC-TRPV4$^{+/+}$ or NSC-TRPV4 cKO mice (Fig. 2C) with *Cx3cr1–green fluorescent protein (GFP)* heterozygous mice, in which microglia are labeled with GFP (Fig. 5D). We found that phagocytic microglia with bulbous tips incorporated the colocalized portions of NSCs and externalized PS (Fig. 5, E to H, and movie S2), which supports the idea that externalized PS mediates the microglial engulfment of NSCs.

Last, we examined whether activation of TRPV4 in NSCs by hyperthermia is sufficient for the engulfment of NSCs by microglia. For this purpose, we performed ex vivo live imaging and pharmacological experiments using acute brain slices containing NSCs and microglia that express tdTomato and GFP, respectively. First, to directly examine the effect of increased temperature on phagocytosis, we visualized the interaction between NSCs and microglia in brain slices incubated in normothermic (35°C) or hyperthermic (38°C) condition for 1 hour (Fig. 6A) and compared microglial engulfment of NSCs (Fig. 6B and movie S3). We found that hyperthermic conditions increased microglial engulfment of NSCs (Fig. 6C). The engulfment of NSCs was significantly suppressed in the presence of HC-067047 (HC; 1 μM), a TRPV4-selective antagonist, while the TRPV4-selective agonist GSK1016790A (5 μM) alone promoted microglial engulfment of NSCs (Fig. 6C). These results indicate that TRPV4 activation enhances microglial engulfment. Furthermore, the effects of hyperthermia and GSK1016790A were blocked by specifically deleting TRPV4 in NSCs (Fig. 6D). These results suggest that hyperthermia enhances microglial engulfment of NSCs in a TRPV4-dependent manner.

To confirm that recognition of externalized PS is required for the engulfment of NSCs by microglia, we examined the effect of blocking externalized PS with recombinant annexin V (AxV), which binds to externalized PS, by ex vivo live imaging. Treatment with recombinant AxV tended to inhibit the enhancement of engulfment by GSK1016790A-induced TRPV4 activation (Fig. 6E). Together, these results suggest that the activation of TRPV4 in NSCs promotes microglial engulfment of NSCs via externalized PS recognition.

DISCUSSION

It remained unclear whether and how the activation of thermosensitive proteins influences SDS-induced dysfunction of hippocampal neurogenesis. Here, we clarified how the activation of thermosensitive TRPV4 in the NSCs affects neurogenesis through temporal- and cell type–specific TRPV4 deletion. In TRPV4 KO and NSC-TRPV4 cKO mice, SDS-induced impairment of neurogenesis was suppressed, suggesting that SDS activates TRPV4 and induces stress responses. These results indicate that temperature is an important

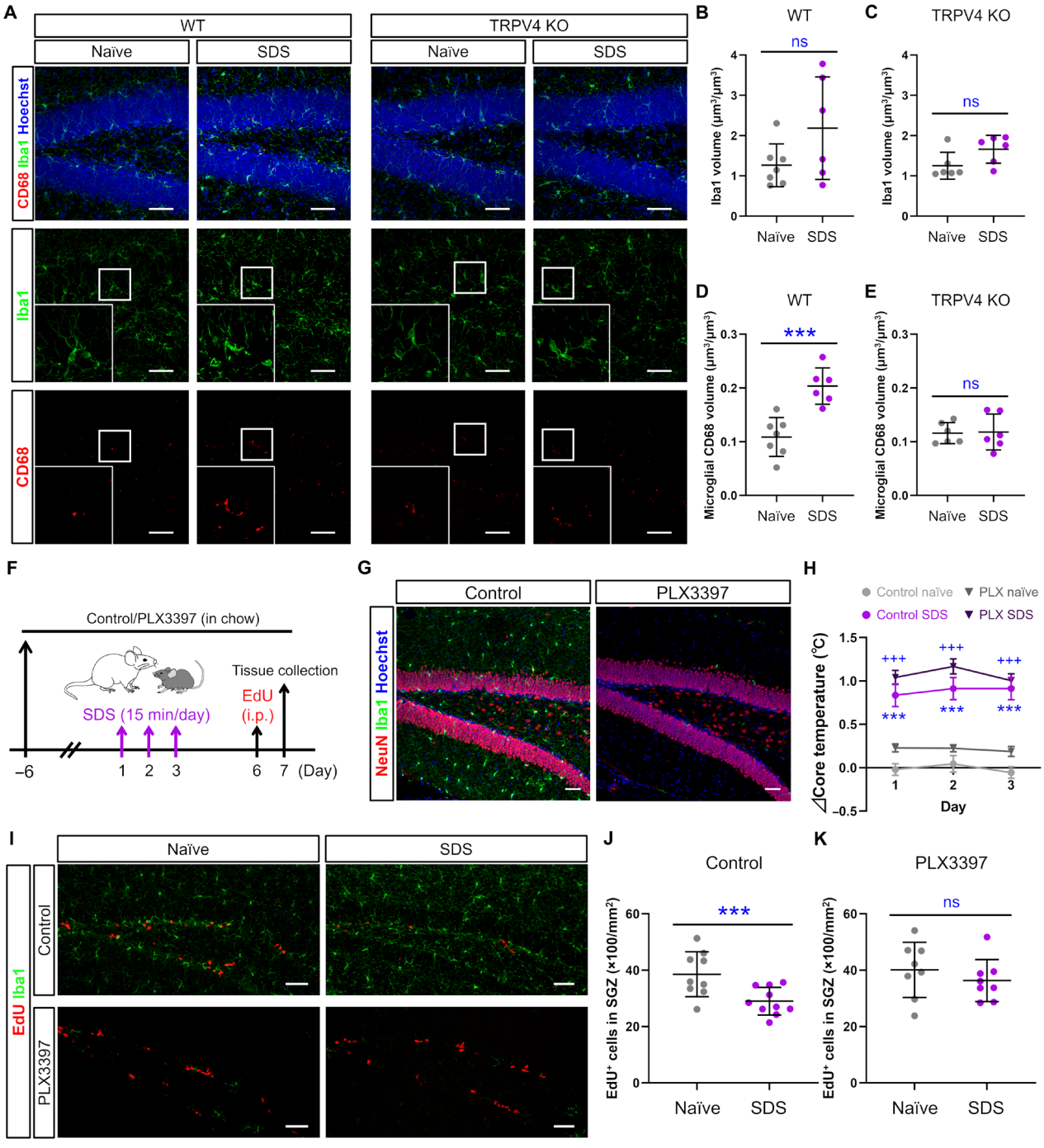

Fig. 3. Microglia mediate SDS-induced impairment of hippocampal neurogenesis. (**A**) Representative confocal images showing Iba1 (microglia) and CD68 (lysosomes) staining in the DG. Scale bars, 50 μm. (**B** and **C**) Comparison of Iba1 staining volume after SDS. $n = 7$ (naïve WT), 6 (SDS-exposed WT), 6 (naïve TRPV4 KO), and 6 (SDS-exposed TRPV4 KO) mice; four areas from two to three sections from each mouse. (**D** and **E**) TRPV4 deficiency suppressed the SDS-induced increase in microglial CD68 volume. $n = 7$ (naïve WT), 6 (SDS-exposed WT), 6 (naïve TRPV4 KO), and 6 (SDS-exposed TRPV4 KO) mice; four areas from two to three sections from each mouse. All n values refer to the number of mice used. $^{***}P < 0.001$ versus naïve WT mice, Student's t test. Data are means ± SEM. (**F**) Schedule of histological analysis following microglial depletion using PLX3397. (**G**) Confocal images indicating that microglia (Iba1), but not neurons (NeuN), were depleted in the DG in PLX3397-treated mice. Scale bars, 50 μm. (**H**) SDS-induced hyperthermia was observed in PLX3397-treated mice. $n = 26$ (control-treated naïve), 25 (control-treated SDS-exposed), 17 (PLX3397 naïve), and 25 (PLX3397 SDS-exposed) mice. (**I**) Representative confocal images of EdU-labeled cells (red) and microglia (Iba1-positive; green) in the SGZ of the DG. Scale bars, 50 μm. (**J** and **K**) The density of newborn cells in the SGZ was decreased in SDS-exposed control-treated mice. This decrease was not observed in PLX3397-treated mice. $n = 9$ (control-treated naïve), 10 (control-treated SDS-exposed), 8 (PLX3397 naïve), and 9 (PLX3397 SDS-exposed) mice. All n values refer to the number of mice used. $^{***}P < 0.001$ versus naïve WT mice; $^{+++}P < 0.001$ versus PLX3397-treated naïve mice, one-way ANOVA followed by Tukey-Kramer's post hoc test (H) or Student's t test (B to E, J, and K). Data are means ± SEM.

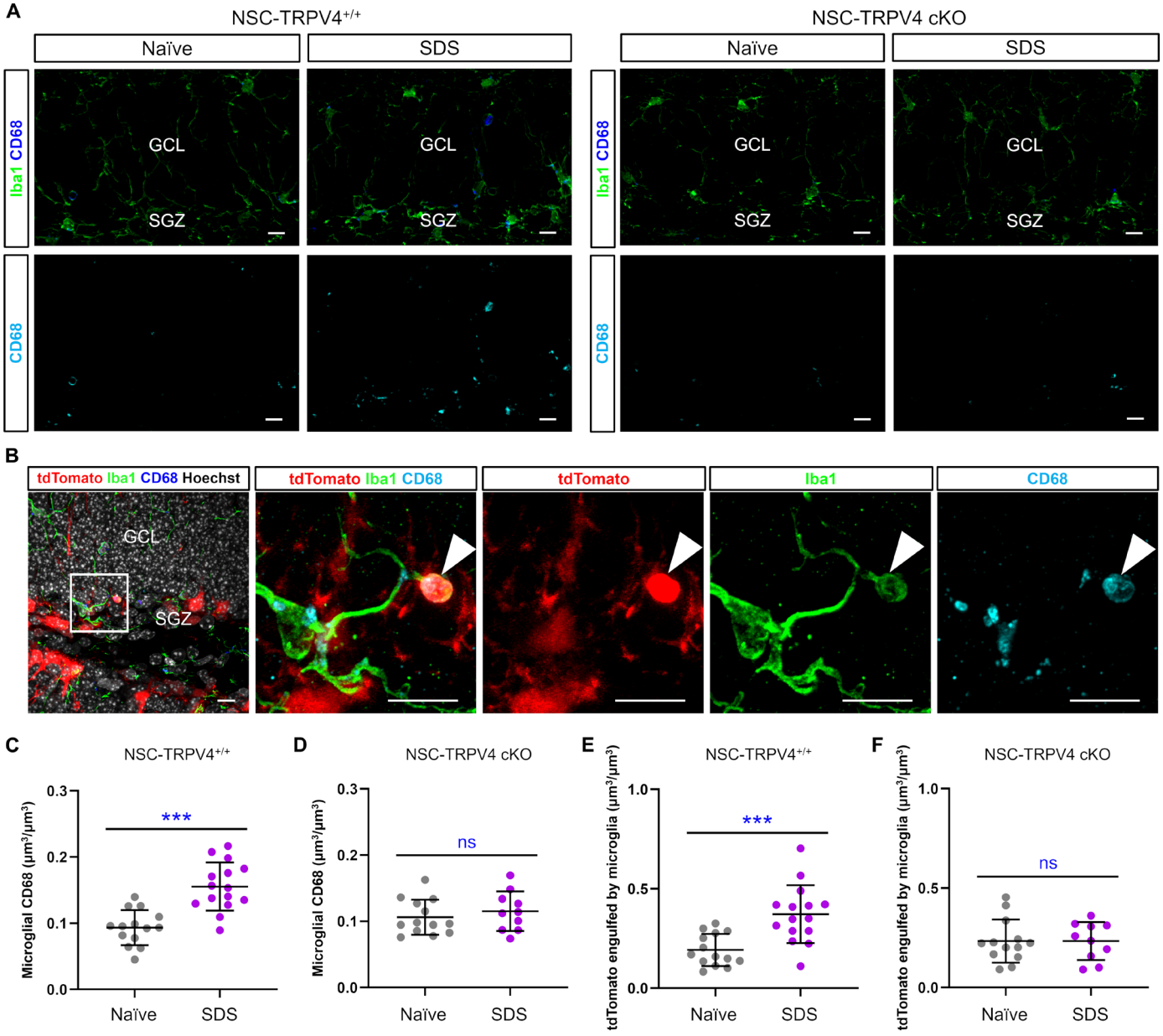

Fig. 4. SDS promotes microglial engulfment of NSCs through TRPV4 activation. (**A**) Representative confocal images showing Iba1 (microglia) and CD68 (lysosomes) staining in the DG. Scale bars, 10 μm. (**B**) Representative confocal images showing engulfed (Iba1 and CD68 double-positive) NSCs (tdTomato; red) in the DG in an NSC-TRPV4$^{+/+}$ mouse after SDS. The white arrowheads indicate microglial lysosomes containing NSCs. Scale bars, 10 μm. (**C** and **D**) Quantitative analysis of Iba1 and CD68 immunostaining in the DG in NSC-TRPV4$^{+/+}$ and NSC-TRPV4 cKO mice 4 days after the last SDS exposure. $n = 14$ (naïve NSC-TRPV4$^{+/+}$), 15 (SDS-exposed NSC-TRPV4$^{+/+}$), 13 (naïve NSC-TRPV4 cKO), and 10 (SDS-exposed NSC-TRPV4 cKO) mice. (**E** and **F**) Microglial engulfment of NSCs was promoted 4 days after the last SDS exposure. $n = 14$ (naïve NSC-TRPV4$^{+/+}$), 15 (SDS-exposed NSC-TRPV4$^{+/+}$), 13 (naïve NSC-TRPV4 cKO), and 10 (SDS-exposed NSC-TRPV4 cKO) mice. All n values refer to the number of mice used. ***$P < 0.001$ versus naïve NSC-TRPV4$^{+/+}$ mice, Student's t test. Data are means ± SEM.

factor mediating the stress response. In previous studies, the cellular and molecular mechanisms that link stress with impairment of adult neurogenesis have mainly focused on diffusion of signaling molecules induced by stress, such as stress hormone, cytokine, and neurotrophic factors (*24*). In the current study, we did not examine whether these molecules contribute to TRPV4 activation or microglial engulfment. However, because hyperthermia alone promoted engulfment of NSCs even in acute brain slices, it is possible that TRPV4 is directly activated by hyperthermia after SDS. In addition, it should be noted that it remains to be determined whether overexpression of TRPV4 could up-regulate Ca^{2+} signaling and control neurogenesis.

We have previously shown that the physiological brain temperature constitutively activates TRPV4 (*10*). In addition, fever additively activated TRPV4 channels in response to an increase in temperature

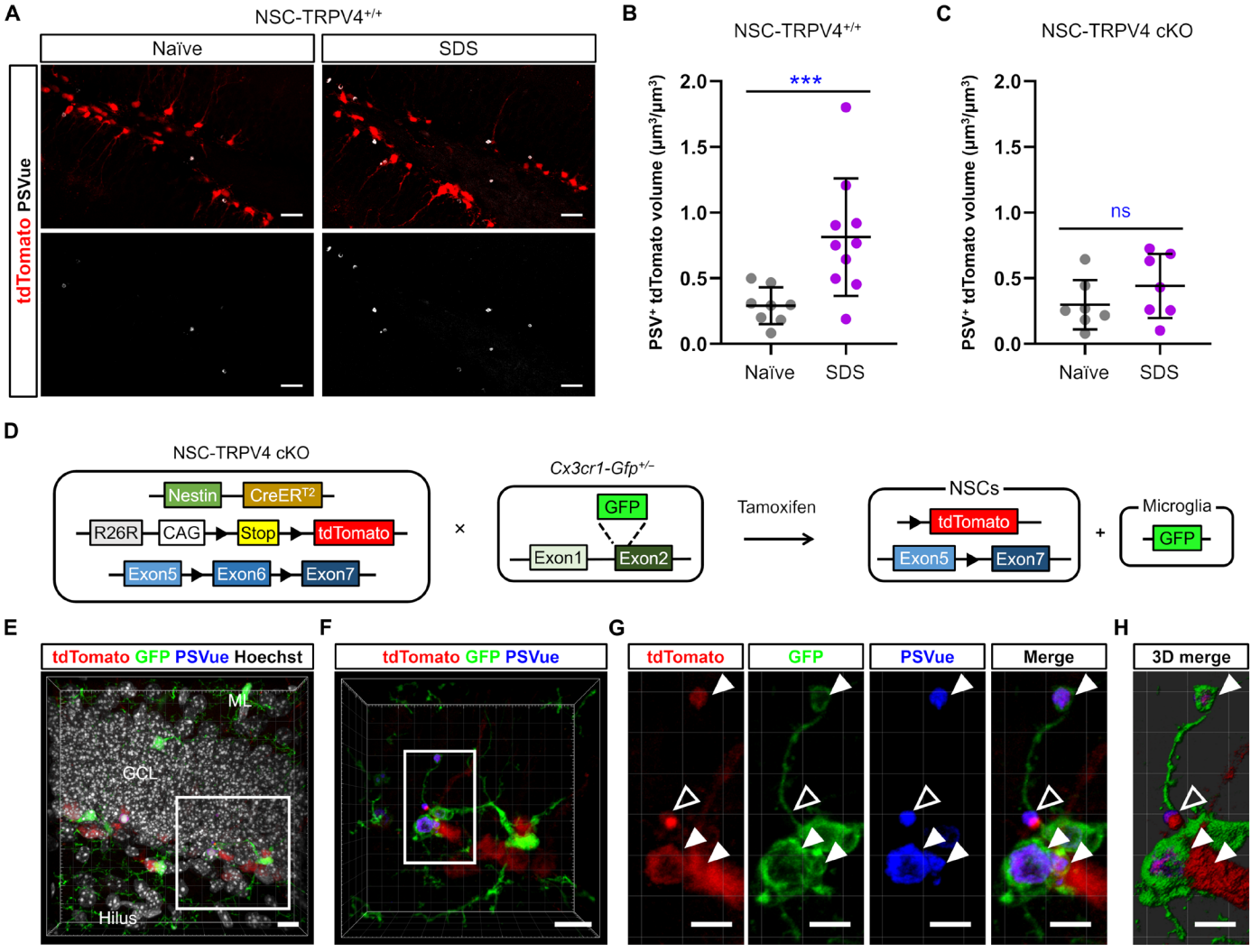

Fig. 5. Microglia engulf NSCs through the recognition of externalized PS. (**A**) Representative confocal images of tdTomato-positive NSCs (red) labeled with PSVue (gray). PS was externalized on NSCs in the DG, especially in the SGZ. Scale bars, 50 μm. (**B** and **C**) SDS-induced increase in externalized PS in NSCs in vivo. The increase in externalized PS was suppressed in NSC-TRPV4 cKO mice. $n = 5$ (naïve NSC-TRPV4$^{+/+}$), 6 (SDS-exposed NSC-TRPV4$^{+/+}$), 6 (naïve NSC-TRPV4 cKO), and 6 (SDS-exposed NSC-TRPV4 cKO) mice; four areas from two to three sections from each mouse. ***$P < 0.05$ versus naïve NSC-TRPV4$^{+/+}$ mice, Student's t test. Data are means ± SEM. (**D**) Breeding strategy for fluorescently labeling NSCs (tdTomato) and microglia (GFP) and simultaneously deleting TRPV4. (**E**) Confocal image of the DG of an SDS-exposed NSC-TRPV4$^{+/+}$::CX3CR1-GFP$^{+/−}$ mouse showing NSCs (tdTomato; red), microglia (GFP; green), and externalized PS (PSVue; blue). Scale bar, 10 μm. (**F**) Higher magnification of the boxed area in (E). Scale bar, 10 μm. (**G**) Higher magnification of the boxed area in (F). The closed arrowheads indicate NSCs with externalized PS (tdTomato$^+$GFP$^+$PSVue$^+$) engulfed by microglia. The open arrowheads indicate externalized PS on NSCs not engulfed by microglia. Scale bars, 5 μm. (**H**) Three-dimensional (3D) reconstruction of the boxed area in (F).

in vivo (*25*). It has been shown that 0.2° to 2°C changes in brain temperature significantly affect brain functions and neuronal properties (*8*). Furthermore, we found that 1°C hyperthermia could exacerbate epilepsy in vivo through the TRPV4 overactivation (*26*). Thus, we speculate that such a seemingly small temperature change increases TRPV4 activity and affects physiological responses in vivo.

The expression of TRPV4 in NSCs suggests that NSCs use TRPV4 as a molecular sensor to respond to external stimuli, including elevated temperature, and to modulate their responses to these stimuli to be accurately integrated into neural circuits. We also found that TRPV4 is expressed in NSCs in subventricular zone and olfactory bulb (fig. S7), suggesting the possibility that TRPV4 activation could also modulate neurogenesis in these regions. Previous findings showing that TRPV4 regulates the fate of mesenchymal stem cells through volume expansion (*27*) and that TRPV channels mediate spontaneous Ca^{2+} signaling in neural stem/progenitor cells (*28*, *29*) support this hypothesis. In addition, it is possible that TRPV4 also controls neurogenesis through mechanical stimuli, because cell proliferation is accompanied by transformation of cell membrane. It has been shown that TRPV4 could control osteogenesis in response to volume expansion (*27*).

Previous studies have shown that hyperthermia affects the function of NSCs in vitro (*30*, *31*), but the underlying molecular mechanisms remain unknown. In addition, during development, neurogenesis is disturbed by heat stress through transient receptor potential channel

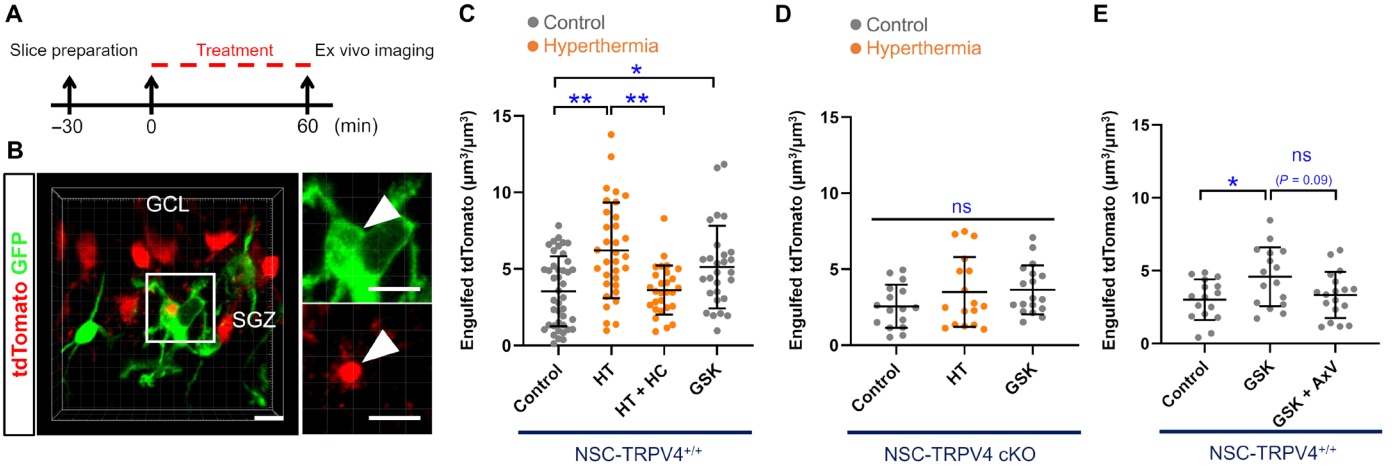

Fig. 6. TRPV4 activation promotes microglial engulfment of NSCs. (**A**) Schedule for ex vivo imaging of NSCs and microglia. (**B**) Representative images of microglial engulfment of NSCs in acute brain slices. The white arrowheads indicate NSCs engulfed by microglia. Scale bars, 10 μm. (**C**) Quantitative analysis of tdTomato engulfed by microglia in slices prepared from NSC-TRPV4$^{+/+}$ mice. $n = 42$ (in slices from control-treated mice), 33 [in slices from hyperthermia (HT)–exposed mice], 28 (in slices from hyperthermia-exposed and HC-067047 (HC)–treated mice], and 28 [in slices from GSK1016790A (GSK)–treated mice] areas; four independent experiments. (**D**) Quantitative analysis of tdTomato engulfed by microglia in slices prepared from NSC-TRPV4 cKO mice. $n = 16$ (in slices from control-treated mice), 17 (in slices from hyperthermia-exposed mice), and 18 (in slices from GSK1016790A-treated mice) areas; four independent experiments. (**E**) Coapplication of AxV and GSK1016790A inhibited microglial engulfment of NSCs ex vivo. $n = 16$ (in slices from vehicle-treated mice), 16 (in slices from GSK1016790A-treated mice), and 18 (in slices from GSK1016790A + rAxV–treated mice) areas; three independent experiments. *$P < 0.05$ and **$P < 0.01$, one-way ANOVA followed by Tukey-Kramer's post hoc test. Data are means ± SEM.

M2 (*32*). Thus, future studies are necessary to further determine the role of heat and TRP receptors in the development and function of stem cells.

It should be noted that the present study does not exclude the possibility that microglial TRPV4 is also a driver of phagocytic removal of newborn neurons, although TRPV4 expression in microglia was lower than that of NSCs in the DG (fig. S4C). Furthermore, because several studies have suggested that microglia can express Nestin (*33*, *34*), it is possible that our Nestin-dependent cKO system could also affect microglial expression of TRPV4. In NSC-TRPV4$^{+/+}$ mice, however, we could hardly see any expression of tdTomato in microglia (fig. S8). Therefore, under the present experimental conditions, the effect of Nestin-dependent TRPV4 cKO on TRPV4 expression in microglia cannot be ruled out, but it is likely less than the effect on TRPV4 expression in NSCs. Last, if microglial TRPV4 is involved in the SDS-induced hyperthermia-dependent impaired neurogenesis reported here, the following possibilities may be considered. For example, microglial TRPV4 is activated by SDS-induced hyperthermia, inducing inflammatory factor release because previous studies have shown that microglial TRPV4 can regulate their reactivity and inflammation (*35*, *36*), which, in turn, induces PS presentation by NSC, leading to engulfment.

Stress is known to induce changes in microglial state and stimulate the release of inflammatory cytokines and chemokines, which adversely affect neurogenesis (*37*, *38*), from microglia (*39*). Furthermore, microglial alteration and suppression of adult neurogenesis are regulated through interleukin-1 receptor under chronic unpredictable stress (*40*). Hence, it is thought that microglia indirectly regulate neurogenesis through cytokine release during stress, but the mechanisms by which microglia regulate neurogenesis regulation under stress remain unclear. Here, we show that microglia directly engulf NSCs in response to SDS, suggesting that excessive engulfment of NSCs by microglia leads to neurogenesis impairment.

The phenomenon that SDS reduces the number of NSCs in the DG has rarely been reported; rather, other stress studies have shown that inflammation reduces the rate of neurogenesis (*37*–*40*). In contrast, our results suggest that microglial engulfment of NSCs reduces the number of NSCs, leading to impaired neurogenesis. Furthermore, recent studies have shown that stress would affect not only the rate of neurogenesis but also the number of NSCs (*41*, *42*), supporting our findings. However, our results do not exclude the possibility that impaired neurogenesis was caused by both microglial engulfment of NSCs and the inflammatory events. Furthermore, microglial engulfment could affect the rate of neurogenesis. Thus, our results suggest that there are cases in which the number of NSCs is reduced by phagocytosis and the rate of neurogenesis remains unchanged, and cases in which the number of NSCs is reduced by phagocytosis and the rate of neurogenesis is also reduced either by microglial engulfment or by inflammatory events (fig. S9). Furthermore, it should be noted that microglia can also induce neurogenesis under certain conditions, such as seizure-induced neurogenesis (*43*), indicating the dual role of microglia on neurogenesis.

It is possible that temperature could affect the differentiated cells that have left the stem cell cycle because mature neurons express TRPV4. Our histological data indicate that TRPV4 is expressed generally in the granule cell layer of DG (Fig. 2A and fig. S4A), suggesting that both mature and immature neurons could sense temperature through TRPV4, although we found externalized PS mainly in SGZ.

In addition, we have shown that the engulfment of NSCs by microglia is mediated by externalized PS recognition, indicating that this so-called eat me signal is involved in the stress response. This process of the engulfment of NSCs is distinctly different from the engulfment of neural precursor cells and viable oligodendrocyte progenitors by microglia during development, which does not involve PS expression on the cell surface (*44*, *45*). It remains unclear how activation of TRPV4 in NSCs leads to interaction with microglia. It is possible

that surveillance of environment by the ramified process of microglia directly recognizes PS on NSCs through PS receptors such as Tyro3/Axl/Mer receptors (*46*). Although not significant, our results also support this hypothesis, as microglial phagocytosis by TRPV4 agonists tends to be inhibited by the PS-binding protein AxV. PS has been shown to be externalized through intracellular Ca^{2+} upregulation (*21*). Because TRPV4 is a Ca^{2+}-permeable channel, it is reasonable that PS exposure is associated with elevated Ca^{2+} via activation of TRPV4 activation.

It is also possible that some factors such as hyperactivity of NSCs and ATP (adenosine 5′-triphosphate) release promote interaction with microglia. In addition, although previous studies have shown that hippocampal neuronal hyperactivity promotes NSC depletion by inducing NSC activation and conversion into astrocytes, thereby impairing neurogenesis (*47*), this phenomenon of NSC-microglia interaction remains unresolved. Elongation of microglial protrusions and cell migration are caused by chemotaxis, which follows a concentration gradient of chemoattractants. If ATP or ADP (adenosine 5′-diphosphate) released by NSCs acts as a chemoattractant, microglia will sense it with purinergic receptors such as P2Y12 and P2X4 receptors, as well as adenosine A1 and A3 receptors (*48*).

Collectively, we establish the critical role of the thermosensitive TRPV4 in NSCs under stress. We revealed a mechanism between stress-induced hyperthermia and impaired hippocampal neurogenesis through microglial engulfment of NSCs. This study would highlight temperature signal and involvement of thermosensitive channels in the regulation of neurogenesis and provide insights for a better understanding of stress response.

MATERIALS AND METHODS

Animal ethics

The experiments were performed with the approval of the Animal Experiment Ethics Committee of the University of Tokyo (approval number: P29-15) and according to the University of Tokyo's guidelines for the care and use of laboratory animals. C57BL/6J mice (male, 3 weeks old) were purchased from SLC Japan Inc. *Trpv4* KO (TRPV4 KO) mice were used in previous studies (*49*). We used the 28th generation of TRPV4 KO mice, which had been backcrossed with C57BL/6J mice at every 5th generation. *Nestin-CreER^{T2}* mice were initially purchased from The Jackson Laboratory (JAX stock #016261) (*50*). *RCL-tdTomato* (JAX stock #007908) and floxed-*Trpv4* (*Trpv4$^{fl/fl}$*) mice were described previously (*51*). To knock out TRPV4 and express tdTomato specifically in NSCs, *RCL-tdTomato* and *Trpv4$^{fl/fl}$* mice were crossed with *Nestin-CreER^{T2}* mice to generate *Nestin-CreER^{T2}::RCL-tdTomato::Trpv4$^{fl/fl}$* mice. *Cx3cr1$^{GFP/GFP}$* mice were purchased from The Jackson Laboratory (JAX stock #005582) (*52*). *Cx3cr1$^{GFP/GFP}$* mice were crossed with *Nestin-CreER^{T2}::RCL-tdTomato::Trpv4$^{fl/fl}$* mice to generate *Nestin-CreERT2::RCL-tdTomato::Trpv4$^{fl/fl}$::Cx3cr1$^{GFP/−}$* mice. All mice were maintained at a controlled temperature on a light schedule and provided access to unlimited food and water. To activate Cre recombinase activity, the mice were fed chow containing tamoxifen (500 mg/kg) (added to AIN-76A standard chow, Research Diets Inc.), as previously described, with minor modifications (*53*) from 3 to 4 weeks (seven consecutive days) after birth. Polymerase chain reaction (PCR) using genomic DNA and previously published primers was used for genotyping (*49*–*52*).

Social defeat stress

Adult male mice were randomly assigned to either the SDS or naïve group. ICR mice (Slc:ICR, 8 to 10 weeks old, purchased from SLC Japan Inc.) were scored as "aggressor" if they exhibited mounting behavior in the first 3 min on all three consecutive days when placed in the novel cage with a novel C57BL/6J mouse, as previously described (*13*), with slight modifications. Singly housed male mice (4 weeks old) were subjected to social defeat by placing them in a novel cage with a male ICR mouse for 15 min each day. We chose three defeat sessions to reduce potential generalization or habituation to the stress exposure, as previously described (*14*). The ICR stressor mouse was placed in the cage 15 min before the SDS session to allow it to become familiar with the novel environment. Because stressor mice were much larger and more dominant than the defeated mice, the defeated mice did not attack the stressor ICR mice. In cases in which social defeat led to the development of wounding (exceeding 0.5 cm), the injured mouse was removed from the study to avoid the possible complex outcomes induced by inflammation that make the interpretation of data difficult. Naïve mice were group-housed (two to three mice per cage) to prevent social isolation stress (*54*) and treated in the same manner in the absence of stressor mice.

Surgery for brain temperature recording

Mice were anesthetized with isoflurane on a stereotactic apparatus (Narishige), and a BF/OT/E Tempfiber probe (Oxford Optronix Ltd.) was implanted. Probe implantation coordinates were −2.1 ± 0.1 mm anteroposterior, ±1.5 mm lateromedial, and −2.0 ± 0.1 mm dorsoventral (from bregma). A drill was used to make a hole (not exceeding 0.5 mm) in the skull for probe implantation. After probe placement, the probe was affixed to the skull with adhesive cement to avoid heat dissipation. The interval between implantation and recording was 10 to 15 min (recovery time for mice), and brain temperature recording was performed within 1 hour. After recording the brain temperature, the mice were perfused transcardially, and the brain samples were fixed followed by the brain section preparation. The cell nuclei of the brain sections were then stained with Hoechst 33342 (1:1000; Thermo Fisher Scientific; overnight) to confirm that the probe was placed in the hippocampus in all mice used for the analysis.

Elevated plus maze test

Mice were placed in a four-arm plus maze with two open and two closed arms (25 cm by 8 cm) 25 cm above the ground for 10 min. These four arms were identical in size, but the closed arms were equipped with 25-cm-high walls at both the sides and the far end. The floorboard was made of white plastic, and the walls were made of opaque gray plastic. The movements of the mice during the 10-min period were recorded by a camera positioned above the maze. Manual scoring was performed to quantify the time spent in protected (body in a closed arm) and unprotected (body in an open arm) areas as a measure of risk assessment, with a blinded observer. To prevent participation in other behavioral tests from influencing the results of later tests, we conducted the EPMT first.

Tail suspension test

Mice were suspended by their tails from a metal rod (30 cm above the floor) for 5 min. Immobility time was measured manually with a blinded observer. To prevent participation in earlier behavioral tests from influencing the results of later tests, we conducted the TST last.

Rectal/body temperature measurement

Core temperature was measured using a RET-4 thermocouple sensor, Type T rectal probe (Physitemp Instruments), and BAT10 thermometer (Physitemp Instruments). Whole-body surface temperature was measured using an infrared thermal camera (T650sc, FLIR Systems). Images were taken at the specified time points.

Sample preparation and immunostaining

Experimental mice were anesthetized with isoflurane and perfused transcardially with cold 0.1 M phosphate-buffered saline (PBS), followed by 4% paraformaldehyde (PFA). The brain samples were postfixed with 4% PFA at 4°C for 24 hours. Coronal sections (100 μm thick) were prepared with a Zero-1 vibratome (Dosaka). The fixed slices were rinsed three times with PBS and incubated in PBS, 0.3% Triton X-100, and 5% goat serum at room temperature for 15 min with agitation. The samples were subsequently incubated with primary antibodies in PBS, 0.3% Triton X-100, and 5% goat serum overnight at room temperature with agitation. After antibody incubation, the slices were rinsed three times with PBS and then incubated with secondary antibodies in PBS, 0.3% Triton X-100, and 5% goat serum for 4 hours at room temperature with agitation. Last, the samples were rinsed three times with PBS, and images were obtained with an FV1200 confocal microscope (Olympus) at 1024 × 1024 pixels using three-line averaging. The stacked images were prepared using ImageJ. Z-series images were collected in 1.00-μm (for 10× and 20× objective lenses) or 0.33-μm (for 40×, 60×, and 100× objective lenses) steps and analyzed using ImageJ. Immunostaining was quantified using a previously described method with minor modifications (*55*). Colocalization was established by stacking 31 z-series images acquired at a *z* step of 0.33 μm. For each z-series image acquired, background was subtracted from all fluorescence channels using ImageJ. To measure the volume of engulfed NSCs, any fluorescence that was not within microglial CD68 volume was subtracted from the image. The remaining engulfed NSC fluorescence volume within CD68 was calculated.

EdU labeling and detection

Three days after the last SDS exposure, the mice received an injection of EdU (50 mg/kg, intraperitoneally; Thermo Fisher Scientific) to label dividing cells. Twenty-four hours after injection, the animals were perfused transcardially with cold PBS followed by 4% PFA in 0.1 M PBS, and the brains were quickly removed, placed in 4% PFA, and postfixed overnight. Coronal sections of the hippocampus (100 μm thick) were prepared using a Zero-1 vibratome (Dosaka). The hippocampal sections were incubated in PBS, 0.3% Triton X-100, and 5% goat serum at room temperature for 15 min with agitation and washed with PBS. The tissues were subjected to the "Click-iT" reaction according to the manufacturer's instructions (Thermo Fisher Scientific) to fluorescently label incorporated EdU with Alexa Fluor 594 or 647 for signal detection.

Reagents

The selective TRPV4 antagonist HC-067047 (2-methyl-1-[3-(4-morpholinyl)propyl]-5-phenyl-*N*-[3-(trifluoromethyl)phenyl]-1*H*-pyrrole-3-carboxamide) and agonist GSK1016790A ([(*N*-((1*S*)-1-{[4-((2*S*)-2-{[(2,4-dichlorophenyl)sulfonyl]amino}-3-hydroxypropanoyl)-1-piperazinyl]carbonyl}-3-methylbutyl)-1-benzothiophene-2-carboxamide]) were purchased from Sigma-Aldrich. AxV recombinant protein (rAxV) was purchased from Thermo Fisher Scientific. rAxV was dissolved in artificial cerebrospinal fluid (ACSF) at a concentration of 10 μg/ml.

Antibodies for immunostaining

We used the following primary antibodies: mouse anti-NeuN (1:500; Millipore, #MAB377), rabbit anti-Iba1 (1:500; Wako, #019-19741), guinea pig anti-Iba1 (1:500; Synaptic Systems, #234 004), guinea pig anti-DCX (1:500; EMD Millipore, #AB2253), rabbit anti-Prox1 (1:500; BioLegend, #PRB-238C), mouse anti-S100β unit (1:500; Sigma-Aldrich, #S2532), rat anti-Nestin (1:500; Abcam, #ab6142), rat anti-CD68 (1:500; Bio-Rad, #MCA1957GA), rat anti-GFP (1:1000; Nacalai Tesque, #04404-26), and rabbit anti-TRPV4 (1:500; generated in this study).

We used the following secondary antibodies: horseradish peroxidase (HRP)–conjugated anti-rabbit immunoglobulin G (IgG) (1:500; Cell Signaling Technology, #7074S); donkey anti-rabbit IgG (H+L) highly cross-adsorbed secondary antibody, Alexa Fluor 546 (1:500; Thermo Fisher Scientific, #A10040); goat anti-rat IgG (H+L) cross-adsorbed secondary antibody, Alexa Fluor 488 (1:500; Thermo Fisher Scientific, #A11006); goat anti-rat IgG (H+L) cross-adsorbed secondary antibody, Alexa Fluor 647 (1:500; Thermo Fisher Scientific, #A21247); goat anti-rabbit IgG (H+L) cross-adsorbed secondary antibody, Alexa Fluor 488 (1:500; Thermo Fisher Scientific, #A11008); goat anti-rabbit IgG (H+L) cross-adsorbed secondary antibody, Alexa Fluor 647 (1:500; Thermo Fisher Scientific, #A21244); goat anti–guinea pig IgG (H+L) highly cross-adsorbed secondary antibody, Alexa Fluor 647 (1:500; Thermo Fisher Scientific, #A21450); and goat anti-mouse IgG (H+L) cross-adsorbed secondary antibody, Alexa Fluor 647 (1:500; Thermo Fisher Scientific, #A21235).

Generation of a TRPV4 antibody

To make an anti-rabbit TRPV4 antibody, a peptide encoding the predicted C terminus of TRPV4 (DGHQQGYAPKWRAEDAPL) was coupled to keyhole limpet hemocyanin and used to immunize rabbits. The immunized rabbit serum was affinity-purified by a peptide-labeled column. To assess the quality of the TRPV4 antibody, immunostaining and immunoblotting experiments were performed in human embryonic kidney (HEK) 293 cells expressing TRPV4. HEK293 cells were cotransfected with mouse TRPV4/pCAG (1 μg/ml) and enhanced GFP/pCAG (0.1 μg/ml) using Lipofectamine 2000 reagent (Invitrogen). For immunostaining, the cells were fixed in 4% PFA in PBS for 10 min. The cells were washed three times with PBS–Tween 20 (PBS-T) and blocked in 3% bovine serum albumin in PBS-T at room temperature for 1 hour. The cells were then incubated with primary antibodies at 4°C overnight. The following antibodies were used: rabbit anti-TRPV4 (1:2000) and rat anti-GFP (1:1000; Nacalai Tesque). After washing with PBS-T, the cells were incubated with the following secondary antibodies: Alexa Fluor 546–conjugated donkey anti-rabbit IgG (1:500; Thermo Fisher Scientific) and Alexa Fluor 488–conjugated goat anti-rat IgG (1:500; Thermo Fisher Scientific). All fluorescence images were captured with a fluorescence microscope (BZ-9000, Keyence). For immunoblotting, membrane fractions were prepared from whole HEK293 cell lysates or the mouse choroid plexus by ultracentrifugation (100,000*g*, 1 hour, 4°C). Proteins from the membrane fractions were separated by 8% SDS–polyacrylamide gel electrophoresis, and the proteins were transferred to polyvinylidene difluoride membranes. The membranes were blotted with the TRPV4 antibody followed by HRP-conjugated anti-rabbit IgG (Cell Signaling Technology). An

enhanced chemiluminescence (ECL) detection kit (Amersham Biosciences) was used to detect the signal.

Microglia depletion

PLX3397 (Chemgood; C-1271) was added to AIN-76A standard chow by Research Diets Inc. The mice were fed PLX3397 (290 mg/kg) in chow for 1 week as previously described (*56*). Control mice were fed AIN-76A standard chow (Research Diets Inc.).

Acute brain slice preparation and ex vivo live cell imaging

Mice were decapitated under anesthesia with isoflurane, and the brains were immediately immersed in ice-cold ACSF. Coronal slices (400 μm thick) were prepared using a VT1200S vibratome (Leica) in an ice-cold modified ACSF (mACSF) as previously described (*57*). Both ACSF and mACSF were oxygenated with 95% O_2 and 5% CO_2. The slices were allowed to recover for at least 30 min and then submerged in a chamber filled with oxygenated ACSF at 35°C. The ACSF consisted of the following: 127 mM NaCl, 26 mM $NaHCO_3$, 3.5 mM KCl, 1.24 mM KH_2PO_4, 1.4 mM $MgSO_4$, 1.2 mM $CaCl_2$, and 10 mM glucose. The mACSF consisted of the following: 222.1 mM sucrose, 27 mM $NaHCO_3$, 1.4 mM NaH_2PO_4, 2.5 mM KCl, 0.5 mM ascorbic acid, 1 mM $CaCl_2$, and 7 mM $MgSO_4$. For ex vivo live cell imaging, the temperature of the microscope stage was regulated and monitored using an INUBSF-ZILCS instrument (Tokai Hit). Microglia and NSCs in the SGZ of the DG were imaged more than 50 μm below the surface of the slice as previously described (*58*, *59*). At this depth, the NSCs and microglia were morphologically intact and showed no signs of activation for up to 2 hours. Images were obtained with an FV1200 confocal microscope (Olympus) at 1024 × 1024 pixels as 10-μm-deep stacks with a step size of 1.00 μm in the *z* axis. The stacked images were prepared and analyzed using ImageJ, and engulfed tdTomato was calculated as the ratio of the merged volume of tdTomato and GFP.

Externalized PS labeling and detection in fixed brain slices

Brain fixation and tissue collection were performed 2 hours after acute SDS, and externalized PS levels in fixed brain slices were evaluated, as has been done in previous study (*60*). It should be noted that no membrane permeabilization was performed during PSVue labeling in the present study; the colocalization of PSVue with raw fluorescence of unimmunostained GFP and tdTomato was observed in Fig. 5 (E to H) to minimize nonspecific PSVue labeling.

The fixed brain slices (prepared as described above) were rinsed three times with PBS. The samples were subsequently incubated with PSVue® 643 (1:100; Molecular Targeting Technologies) and Hoechst 33342 (1:500; Thermo Fisher Scientific) in PBS overnight at room temperature with agitation. After incubation, the slices were rinsed three times with PBS, and images were obtained with an FV1200 confocal microscope (Olympus) at 1024 × 1024 pixels with three-line averaging. Z-series images were collected in 0.33-μm steps and analyzed using ImageJ.

Experimental design and statistical analysis

MATLAB, Imaris, and Prism software were used to analyze the data and generate graphs in this work. Data were subjected to parametric or nonparametric tests, depending on the results of the test of normality. Minimum sample sizes were estimated from previously published datasets with similar experimental parameters. The data collection, manual scoring for behavior with video recording, cell count, and histological analysis were performed in a blinded manner to avoid bias. The data were statistically analyzed in a blinded manner. The data are presented as means ± SEM.

SUPPLEMENTARY MATERIALS

Supplementary material for this article is available at https://science.org/doi/10.1126/sciadv.abj8080

View/request a protocol for this paper from *Bio-protocol*.

REFERENCES AND NOTES

1. B. R. Miller, R. Hen, The current state of the neurogenic theory of depression and anxiety. *Curr. Opin. Neurobiol.* **30**, 51–58 (2015).
2. A. Denoth-Lippuner, S. Jessberger, Formation and integration of new neurons in the adult hippocampus. *Nat. Rev. Neurosci.* **22**, 223–236 (2021).
3. N. L. S. Machado, S. B. G. Abbott, J. M. Resch, L. Zhu, E. Arrigoni, B. B. Lowell, P. M. Fuller, M. A. P. Fontes, C. B. Saper, A glutamatergic hypothalamomedullary circuit mediates thermogenesis, but not heat conservation, during stress-induced hyperthermia. *Curr. Biol.* **28**, 2291–2301.e5 (2018).
4. N. Kataoka, Y. Shima, K. Nakajima, K. Nakamura, A central master driver of psychosocial stress responses in the rat. *Science* **367**, 1105–1112 (2020).
5. H. Wang, B. Wang, K. P. Normoyle, K. Jackson, K. Spitler, M. F. Sharrock, C. M. Miller, C. Best, D. Llano, R. Du, Brain temperature and its fundamental properties: A review for clinical neuroscientists. *Front. Neurosci.* **8**, 307 (2014).
6. C. L. Tan, Z. A. Knight, Regulation of body temperature by the nervous system. *Neuron* **98**, 31–48 (2018).
7. E. I. Moser, P. Andersen, Conserved spatial learning in cooled rats in spite of slowing of dentate field potentials. *J. Neurosci.* **14**, 4458–4466 (1994).
8. S. F. Owen, M. H. Liu, A. C. Kreitzer, Thermal constraints on in vivo optogenetic manipulations. *Nat. Neurosci.* **22**, 1061–1065 (2019).
9. A. D. Güler, H. Lee, T. Iida, I. Shimizu, M. Tominaga, M. Caterina, Heat-evoked activation of the ion channel, TRPV4. *J. Neurosci.* **22**, 6408–6414 (2002).
10. K. Shibasaki, M. Suzuki, A. Mizuno, M. Tominaga, Effects of body temperature on neural activity in the hippocampus: Regulation of resting membrane potentials by transient receptor potential vanilloid 4. *J. Neurosci.* **27**, 1566–1575 (2007).
11. J. A. Kauer, H. E. Gibson, Hot flash: TRPV channels in the brain. *Trends Neurosci.* **32**, 215–224 (2009).
12. P. Kanju, W. Liedtke, Pleiotropic function of TRPV4 ion channels in the central nervous system. *Exp. Physiol.* **101**, 1472–1476 (2016).
13. S. A. Golden, H. E. Covington III, O. Berton, S. J. Russo, A standardized protocol for repeated social defeat stress in mice. *Nat. Protoc.* **6**, 1183–1191 (2011).
14. T. B. Franklin, B. A. Silva, Z. Perova, L. Marrone, M. E. Masferrer, Y. Zhan, A. Kaplan, L. Greetham, V. Verrechia, A. Halman, S. Pagella, A. L. Vyssotski, A. Illarionova, V. Grinevich, T. Branco, C. T. Gross, Prefrontal cortical control of a brainstem social behavior circuit. *Nat. Neurosci.* **20**, 260–270 (2017).
15. V. Benfenati, M. Amiry-Moghaddam, M. Caprini, M. N. Mylonakou, C. Rapisarda, O. P. Ottersen, S. Ferroni, Expression and functional characterization of transient receptor potential vanilloid-related channel 4 (TRPV4) in rat cortical astrocytes. *Neuroscience* **148**, 876–892 (2007).
16. M. Konno, H. Shirakawa, S. Iida, S. Sakimoto, I. Matsutani, T. Miyake, K. Kageyama, T. Nakagawa, K. Shibasaki, S. Kaneko, Stimulation of transient receptor potential vanilloid 4 channel suppresses abnormal activation of microglia induced by lipopolysaccharide. *Glia* **60**, 761–770 (2012).
17. K. Shibasaki, K. Ikenaka, F. Tamalu, M. Tominaga, Y. Ishizaki, A novel subtype of astrocytes expressing TRPV4 (transient receptor potential vanilloid 4) regulates neuronal excitability via release of gliotransmitters. *J. Biol. Chem.* **289**, 14470–14480 (2014).
18. A. Sierra, J. M. Encinas, J. J. P. Deudero, J. H. Chancey, G. Enikolopov, L. S. Overstreet-Wadiche, S. E. Tsirka, M. Maletic-Savatic, Microglia shape adult hippocampal neurogenesis through apoptosis-coupled phagocytosis. *Cell Stem Cell* **7**, 483–495 (2010).
19. C. Luo, R. Koyama, Y. Ikegaya, Microglia engulf viable newborn cells in the epileptic dentate gyrus. *Glia* **64**, 1508–1517 (2016).
20. M. Colonna, O. Butovsky, Microglia function in the central nervous system during health and neurodegeneration. *Annu. Rev. Immunol.* **35**, 441–468 (2017).
21. S. Nagata, J. Suzuki, K. Segawa, T. Fujii, Exposure of phosphatidylserine on the cell surface. *Cell Death Differ.* **23**, 952–961 (2016).
22. T. Li, B. Chiou, C. K. Gilman, R. Luo, T. Koshi, D. Yu, H. C. Oak, S. Giera, E. Johnson-Venkatesh, A. K. Muthukumar, B. Stevens, H. Umemori, X. Piao, A splicing isoform of GPR56 mediates microglial synaptic refinement via phosphatidylserine binding. *EMBO J.* **39**, e104136 (2020).
23. N. Scott-Hewitt, F. Perrucci, R. Morini, M. Erreni, M. Mahoney, A. Witkowska, A. Carey, E. Faggiani, L. T. Schuetz, S. Mason, M. Tamborini, M. Bizzotto, L. Passoni, F. Filipello,

R. Jahn, B. Stevens, M. Matteoli, Local externalization of phosphatidylserine mediates developmental synaptic pruning by microglia. *EMBO J.* **39**, e105380 (2020).
24. M. Egeland, P. A. Zunszain, C. M. Pariante, Molecular mechanisms in the regulation of adult neurogenesis during stress. *Nat. Rev. Neurosci.* **16**, 189–200 (2015).
25. K. Shibasaki, S. Sugio, K. Takao, A. Yamanaka, T. Miyakawa, M. Tominaga, Y. Ishizaki, TRPV4 activation at the physiological temperature is a critical determinant of neuronal excitability and behavior. *Pflugers Arch.* **467**, 2495–2507 (2017).
26. K. Shibasaki, K. Yamada, H. Miwa, Y. Yanagawa, M. Suzuki, M. Tominaga, Y. Ishizaki, Temperature elevation in epileptogenic foci exacerbates epileptic discharge through TRPV4 activation. *Lab. Invest.* **100**, 274–284 (2020).
27. H. P. Lee, R. Stowers, O. Chaudhuri, Volume expansion and TRPV4 activation regulate stem cell fate in three-dimensional microenvironments. *Nat. Commun.* **10**, 529 (2019).
28. P. J. Morgan, R. Hübner, A. Rolfs, M. J. Frech, Spontaneous calcium transients in human neural progenitor cells mediated by transient receptor potential channels. *Stem Cells Dev.* **22**, 2477–2486 (2013).
29. V. Coronas, E. Terrié, N. Déliot, P. Arnault, B. Constantin, Calcium channels in adult brain neural stem cells and in glioblastoma stem cells. *Front. Cell. Neurosci.* **14**, 600018 (2020).
30. H. Omori, M. Otsu, A. Suzuki, T. Nakayama, K. Akama, M. Watanabe, N. Inoue, Effects of heat shock on survival, proliferation and differentiation of mouse neural stem cells. *Neurosci. Res.* **79**, 13–21 (2014).
31. L. Wang, Y. Deng, D. Duan, S. Sun, L. Ge, Y. Zhuo, T. Yuan, P. Wu, H. Wang, M. Lu, Y. Xia, Hyperthermia influences fate determination of neural stem cells with lncRNAs alterations in the early differentiation. *PLOS ONE* **12**, e0171359 (2017).
32. Y. Li, J. Jiao, Deficiency of TRPM2 leads to embryonic neurogenesis defects in hyperthermia. *Sci. Adv.* **6**, eaay6350 (2020).
33. S. G. Wohl, C. W. Schmeer, T. Friese, O. W. Witte, S. Isenmann, In situ dividing and phagocytosing retinal microglia express nestin, vimentin, and NG2 in vivo. *PLOS ONE* **6**, e22408 (2011).
34. S. Krishnasamy, Y. C. Weng, S. S. Thammisetty, D. Phaneuf, M. Lalancette-Hebert, J. Kriz, Molecular imaging of nestin in neuroinflammatory conditions reveals marked signal induction in activated microglia. *J. Neuroinflammation* **14**, 45 (2017).
35. M. Liu, X. Liu, L. Wang, Y. Wang, F. Dong, J. Wu, X. Qu, Y. Liu, Z. Liu, H. Fan, R. Yao, TRPV4 inhibition improved myelination and reduced glia reactivity and inflammation in a cuprizone-induced mouse model of demyelination. *Front. Cell. Neurosci.* **12**, 392 (2018).
36. Z. Wang, L. Zhou, D. An, W. Xu, C. Wu, S. Sha, Y. Li, Y. Zhu, A. Chen, Y. Du, L. Chen, L. Chen, TRPV4-induced inflammatory response is involved in neuronal death in pilocarpine model of temporal lobe epilepsy in mice. *Cell Death Dis.* **10**, 386 (2019).
37. C. T. Ekdahl, J. H. Claasen, S. Bonde, Z. Kokaia, O. Lindvall, Inflammation is detrimental for neurogenesis in adult brain. *Proc. Natl. Acad. Sci. U.S.A.* **100**, 13632–13637 (2003).
38. M. L. Monje, H. Toda, T. D. Palmer, Inflammatory blockade restores adult hippocampal neurogenesis. *Science* **302**, 1760–1765 (2003).
39. R. Yirmiya, N. Rimmerman, R. Reshef, Depression as a microglial disease. *Trends Neurosci.* **38**, 637–658 (2015).
40. T. Kreisel, M. G. Frank, T. Licht, R. Reshef, O. Ben-Menachem-Zidon, M. V. Baratta, S. F. Maier, R. Yirmiya, Dynamic microglial alterations underlie stress-induced depressive-like behavior and suppressed neurogenesis. *Mol. Psychiatry* **19**, 699–709 (2014).
41. S. Jung, S. Choe, H. Woo, H. Jeong, H. K. An, H. Moon, H. Y. Ryu, B. K. Yeo, Y. W. Lee, H. Choi, J. Y. Mun, W. Sun, H. K. Choe, E. K. Kim, S. W. Yu, Autophagic death of neural stem cells mediates chronic stress-induced decline of adult hippocampal neurogenesis and cognitive deficits. *Autophagy* **16**, 512–530 (2020).
42. P. Bielefeld, M. R. Abbink, A. R. Davidson, N. Reijner, O. Abiega, P. J. Lucassen, A. Korosi, C. P. Fitzsimons, Early life stress decreases cell proliferation and the number of putative adult neural stem cells in the adult hypothalamus. *Stress* **24**, 189–195 (2021).
43. M. Mo, U. B. Eyo, M. Xie, J. Peng, D. B. Bosco, A. D. Umpierre, X. Zhu, D. S. Tian, P. Xu, L. J. Wu, Microglial P2Y12 receptor regulates seizure-induced neurogenesis and immature neuronal projections. *J. Neurosci.* **39**, 9453–9464 (2019).
44. C. L. Cunningham, V. Martínez-Cerdeño, S. C. Noctor, Microglia regulate the number of neural precursor cells in the developing cerebral cortex. *J. Neurosci.* **33**, 4216–4233 (2013).
45. A. D. Nemes-Baran, D. R. White, T. M. DeSilva, Fractalkine-dependent microglial pruning of viable oligodendrocyte progenitor cells regulates myelination. *Cell Rep.* **32**, 108047 (2020).
46. Y. Tufail, D. Cook, L. Fourgeaud, C. J. Powers, K. Merten, C. L. Clark, E. Hoffman, A. Ngo, K. J. Sekiguchi, C. C. O'Shea, G. Lemke, A. Nimmerjahn, Phosphatidylserine exposure controls viral innate immune responses by microglia. *Neuron* **93**, 574–586.e8 (2017).
47. A. Sierra, S. Martín-Suárez, R. Valcárcel-Martín, J. Pascual-Brazo, S.-A. Aelvoet, O. Abiega, J. J. Deudero, A. L. Brewster, I. Bernales, A. E. Anderson, V. Baekelandt, M. Maletić-Savatić, J. M. Encinas, Neuronal hyperactivity accelerates depletion of neural stem cells and impairs hippocampal neurogenesis. *Cell Stem Cell* **16**, 488–503 (2015).
48. S. Koizumi, K. Ohsawa, K. Inoue, S. Kohsaka, Purinergic receptors in microglia: Functional modal shifts of microglia mediated by P2 and P1 receptors. *Glia* **61**, 47–54 (2013).
49. M. Suzuki, A. Mizuno, K. Kodaira, M. Imai, Impaired pressure sensation in mice lacking TRPV4. *J. Biol. Chem.* **278**, 22664–22668 (2003).
50. D. C. Lagace, M. C. Whitman, M. A. Noonan, J. L. Ables, N. A. DeCarolis, A. A. Arguello, M. H. Donovan, S. J. Fischer, L. A. Farnbauch, R. D. Beech, R. J. DiLeone, C. A. Greer, C. D. Mandyam, A. J. Eisch, Dynamic contribution of nestin-expressing stem cells to adult neurogenesis. *J. Neurosci.* **27**, 12623–12629 (2007).
51. R. Gualdani, F. Seghers, X. Yerna, O. Schakman, N. Tajeddine, Y. Achouri, F. Tissir, O. Devuyst, P. Gailly, Mechanical activation of TRPV4 channels controls albumin reabsorption by proximal tubule cells. *Sci. Signal.* **13**, eabc6967 (2020).
52. S. Jung, J. Aliberti, P. Graemmel, M. J. Sunshine, G. W. Kreutzberg, A. Sher, D. R. Littman, Analysis of fractalkine receptor CX_3CR1 function by targeted deletion and green fluorescent protein reporter gene insertion. *Mol. Cell. Biol.* **20**, 4106–4114 (2000).
53. J. C. Cronk, A. J. Filiano, A. Louveau, I. Marin, R. Marsh, E. Ji, D. H. Goldman, I. Smirnov, N. Geraci, S. Acton, C. C. Overall, J. Kipnis, Peripherally derived macrophages can engraft the brain independent of irradiation and maintain an identity distinct from microglia. *J. Exp. Med.* **215**, 1627–1647 (2018).
54. T. Demuyser, L. Deneyer, E. Bentea, G. Albertini, J. V. Liefferinge, E. Merckx, A. De Prins, D. De Bundel, A. Massie, I. Smolders, In-depth behavioral characterization of the corticosterone mouse model and the critical involvement of housing conditions. *Physiol. Behav.* **156**, 199–207 (2016).
55. D. P. Schafer, E. K. Lehrman, A. G. Kautzman, R. Koyama, A. R. Mardinly, R. Yamasaki, R. M. Ransohoff, M. E. Greenberg, B. A. Barres, B. Stevens, Microglia sculpt postnatal neural circuits in an activity and complement-dependent manner. *Neuron* **74**, 691–705 (2012).
56. M. R. Elmore, A. R. Najafi, M. A. Koike, N. N. Dagher, E. E. Spangenberg, R. A. Rice, M. Kitazawa, B. Matusow, H. Nguyen, B. L. West, K. N. Green, Colony-stimulating factor 1 receptor signaling is necessary for microglia viability, unmasking a microglia progenitor cell in the adult brain. *Neuron* **82**, 380–397 (2014).
57. Y. Hoshi, K. Okabe, K. Shibasaki, T. Funatsu, N. Matsuki, Y. Ikegaya, R. Koyama, Ischemic brain injury leads to brain edema via hyperthermia-induced TRPV4 activation. *J. Neurosci.* **38**, 5700–5709 (2018).
58. C. Madry, V. Kyrargyri, I. L. Arancibia-Cárcamo, R. Jolivet, S. Kohsaka, R. M. Bryan, D. Attwell, Microglial ramification, surveillance, and interleukin-1β release are regulated by the two-pore domain K^+ channel THIK-1. *Neuron* **97**, 299–312.e6 (2018).
59. L. P. Bernier, E. M. York, A. Kamyabi, H. B. Choi, N. L. Weilinger, B. A. MacVicar, Microglial metabolic flexibility supports immune surveillance of the brain parenchyma. *Nat. Commun.* **11**, 1559 (2020).
60. J. Kersigo, A. D'Angelo, B. D. Gray, G. A. Soukup, B. Fritzsch, The role of sensory organs and the forebrain for the development of the craniofacial shape as revealed by Foxg1-cre-mediated microRNA loss. *Genesis* **49**, 326–341 (2011).

Acknowledgments
Funding: This work was supported by Grant-in-Aid for Transformative Research Areas (A) "Glia decoding" from Japan Society for the Promotion of Science (JSPS) 20H05897 (to R.K.), Precursory Research for Embryonic Science and Technology from Japan Science and Technology Agency (JST) JPMJPR18H4 (to R.K.), and Exploratory Research for Advanced Technology from Japan Science and Technology Agency (JST) JPMJER1801 (to Y.I.). **Author contributions:** R.K. and Y.H. designed the experiments. Y.H. performed the experiments. R.K., Y.I., and Y.H. analyzed the data. K.S. generated the anti-TRPV4 antibody and contributed to the discussion of the properties of TRPV4. P.G. generated the floxed-TRPV4 ($TRPV4^{fl/fl}$) mouse line. R.K. and Y.I. supervised the project. R.K. and Y.H. wrote the manuscript with contributions from all authors. **Competing interests:** The authors declare that they have no competing interests. **Data and materials availability:** All data needed to evaluate the conclusions in the paper are present in the paper and/or the Supplementary Materials.

Submitted 3 June 2021
Accepted 8 October 2021
Published 26 November 2021
10.1126/sciadv.abj8080